Interaction between 1/2001 dislocations and 110 prismatic loops in uranium dioxide: Implications for strain-hardening under irradiation

Marion Borde, Laurent Dupuy, Adrien Pivano, Bruno Michel, David Rodney, Jonathan Amodeo

Originally published in International Journal of Plasticity, July 2023. Please cite as :
M. Borde, L. Dupuy, A. Pivano, B. Michel, D. Rodney, J. Amodeo, Interaction between 1/2<110>{001} dislocations and {110} prismatic loops in uranium dioxide: Implications for strain-hardening under irradiation, Int. J. Plast. 168 (2023) 103702. https://doi.org/10.1016/j.ijplas.2023.103702.

Interaction between 1/2<110>{001} dislocations and {110} prismatic loops in uranium dioxide: implications for strain-hardening under irradiation

Marion Borde[a,b,c], Laurent Dupuy[f], Adrien Pivano[d], Bruno Michel[c], David Rodney[b] and Jonathan Amodeo[e,*]

[a] *Université Lyon, CNRS, INSA Lyon, UCBL, MATEIS UMR5510, 69621 Villeurbanne, France*

[b] *Institut Lumière Matière, Université Lyon 1 - CNRS, 69622 Villeurbanne, France*

[c] *CEA, DES, IRESNE, DEC, SESC, LSC, 13108 Saint-Paul-Lez-Durance, France*

[d] *CEA, DES, IRESNE, DEC, SESC, LM2C, 13108 Saint-Paul-Lez-Durance, France*

[e] *Aix-Marseille Université, Université de Toulon, CNRS, IM2NP, 13397 Marseille, France*

[f] *Université Paris-Saclay, CEA, Service de Recherches Métallurgiques Appliquées, 91191 Gif-sur-Yvette, France*

ARTICLE INFO

Keywords:

UO_2

dislocations

irradiation loop

molecular dynamics

discrete dislocation dynamics

ABSTRACT

Plasticity of irradiated UO_2 is of major interest to improve the risk assessment of the nuclear fuel cladding failure in the case of design basis accidents. In this study, we investigate the main irradiation-hardening processes induced by {110} irradiation loops interacting with glissile dislocations of the primary slip system, 1/2<110>{001}, of UO_2. The interactions are simulated at two scales using molecular dynamics and discrete dislocation dynamics, to characterise local interactions and identify strengthening configurations as a function of the dislocation-irradiation loop geometry. In particular, we show that 1/2<110>{001} screw dislocations can be strongly pinned by helical turn configurations. Statistical large-scale discrete dislocation simulations are performed to investigate the collective behaviour of a large density of irradiation defects and quantify irradiation hardening. Several microstructural processes including loop drag and shovelling are observed and their involvement in clear band formation and hardening of UO_2 fuel at high temperature is discussed.

1. Introduction

Understanding the mechanical behaviour of nuclear power plant constituents and fuel under nominal, transient, and incidental conditions is of major interest for nuclear safety (Zinkle and Was 2013; Frazer et al. 2021). Uranium dioxide (UO_2, fluorite structure) is the most commonly used fuel in the nuclear industry. During hypothetical accidental operations (last stage of power transient), the temperature in the centre of fuel pellets increases up to ∼2300 K (Michel et al. 2013), which promotes creep deformation and can compromise the fuel integrity. To address the fuel behaviour under these conditions, it has to be considered that UO_2 fuel pellets are subjected to microstructural changes including the formation of point defects such as vacancies, interstitials, Frenkel pairs, *etc.* and extended defects such as bubbles (group of vacancies) that accommodate fission gas products (Baker 1977; Sonoda et al. 2002; Panetier et al. 2022), {110} and {111} prismatic loops that are generated by the accumulation of irradiation-induced interstitial atoms (Whapham 1966; Jonnet et al. 2008; Ye et al. 2011; He et al. 2014; Onofri et al. 2016; Onofri et al. 2017; Onofri et al. 2020). Irradiation defects are known to modify the mechanical stability of crystalline materials. While their effect has been intensively studied in structural metals and alloys (Li et al. 2014; Armstrong et al. 2015; Saleh et al. 2016; Monnet

*Corresponding author
ORCID(s):

2018; Das et al. 2020; Cui et al. 2021), only few studies have investigated the link between the dislocation microstructure and the mechanical behaviour changes (including hardening) induced by the irradiation defects in the fuel. In pristine conditions, the deformation of UO_2 single crystals is characterised by dislocation glide in the 1/2<110>{001} slip system but plasticity activity in 1/2<110>{110} and 1/2<110>{111}, respectively referred as deformation modes I, II and III, is also observed (Byron 1968; Nadeau 1969; Yust and McHargue 1969; Sawbridge and Sykes 1971; Lefèbvre et al. 1976; Alamo et al. 1978; Keller et al. 1988a; Keller et al. 1988b). The deformation of UO_2 single crystals is known to be highly thermally-activated due to the Peierls lattice friction. This latter induces temperature-dependent dislocation glide processes up to a critical temperature $T_c^{\{hkl\}}$, which depends on the deformation mode and above which dislocation-forest interactions as well as high-temperature dislocation processes such as dislocation cross-slip and climb take place. Compressing stoichiometric UO_2 single crystals, Sawbridge and Sykes have shown that mode I and II slip systems can be activated independently, in contrast to mode III for which dislocations are only observed under multi-slip conditions (Sawbridge and Sykes 1971; Keller et al. 1988b). In the lattice friction regime, experimental critical resolved shear stresses (CRSS) are lower in the 1/2<110>{001} slip system, which confirms the easier glide of mode I dislocations when compared to the two other deformation modes (Byron 1968; Nadeau 1969; Sawbridge and Sykes 1971). Dislocation activity in the 1/2<110>{001} slip system was recently confirmed using micro-compression testing (Frazer and Hosemann 2019). Also, Nadeau hypothesises that dislocation glide in the thermally-activated regime proceeds by a kink-pair mechanism (Nadeau 1969) as commonly observed in body-centered cubic (BCC) metals (Rodney and Proville 2009; Naamane et al. 2010; Cereceda et al. 2016) and other cubic metal oxides (Messerschmidt 2010; Amodeo et al. 2011; Amodeo et al. 2016; Portelette et al. 2018). Since then, atomistic simulations have confirmed that the 1/2<110>{001} slip system is the easiest to activate (as in the experiments), both 1/2<110>{110} and 1/2<110>{111} slip systems being characterised by a more significant lattice friction (Fossati et al. 2013; Skelton and Walker 2017). Otherwise, the kink-pair mechanism was confirmed by several numerical studies focusing on the mobility of edge 1/2<110>{001} and screw 1/2<110>{110} dislocations (Lunev et al. 2017; Lunev et al. 2018; Soulié et al. 2018; Borde et al. 2022). Peierls stress (minimum stress to move a dislocation at zero temperature) calculations performed by Skelton and collaborators are consistent with these conclusions (Skelton and Walker 2017). However, less is known about dislocation slip in UO_2 in the athermal regime of deformation ($T>T_c^{\{hkl\}}$). Portelette *et al.* have estimated the athermal transition temperature $T_a^{\{001\}}$ at about 1750 K after post-processing several experimental data sets (Portelette et al. 2018). The same group also investigated the role of dislocation-forest interactions and cross-slip using discrete dislocation dynamics (DDD) but without considering irradiation (Portelette et al. 2020; Madec et al. 2023). Their DDD outputs (interaction matrix coefficients) have recently been integrated into a crystal plasticity framework to investigate polycristalline UO_2 (Lindroos et al. 2023). Absorption of vacancies at screw dislocations was simulated (Liu et al. 2019) but the effect on the mobility was not investigated.

Irradiation-induced dislocations in UO_2 were investigated using transmission electron microscopy (TEM) (Whapham 1966; Jonnet et al. 2008; Onofri et al. 2016; Onofri et al. 2017; Onofri et al. 2020). Irradiation loops are unfaulted and of interstitial type with a Burgers vector along 1/2<110>. The various studies agree that the nucleation and growth of irradiation loops obeys a multi-stage process. First is the nucleation regime where the loop average nucleation size is estimated in the 3-7 nm range (low to intermediate irradiation dose). This stage is characterised by a net increase of the prismatic loop density before it reaches a steady-state, as also described by other authors (Ye et al. 2011; He et al. 2014). Then, the growth and coalescence stages show an increase of the prismatic loop average diameter and the coalescence of the larger loops into dislocation lines (larger irradiation dose). This process was also interpreted as a migration-coalescence process by He *et al.* using *in situ* TEM experiments at ~1100 K (He et al. 2014). Finally, a steady-state regime takes place where the prismatic loop density slightly decreases concomitantly to the nucleation of additional loops lying in-between the dislocation lines. Onofri and collaborators proposed that the coarsening of irradiation loops in UO_2 is due to an Ostwald ripening process characterised by the dissolution of small loops and absorption of interstitial atoms into larger loops (Onofri et al. 2016). Finally, the decrease of the loop density observed within the fourth stage is attributed to the interactions of the prismatic loops with each other as well as with primary dislocations. During this last stage, He *et al.* did not mention any decrease of the prismatic loop diameter (He et al. 2014). Le Prioux *et al.* have investigated the structure of {110} and {111} prismatic loops in UO_2 using atomistic simulations using a rigid-ion model (Le Prioux et al. 2016). {110} unfaulted prismatic loops have proved to be more stable when compared to {111} faulted loops assuming a critical size larger than few tens of UO_2 molecules. An atomic structure of the {110} prismatic loop was also proposed by Onofri *et al.* (Onofri et al. 2017). Molecular dynamics (MD) simulations have been intensively used to study irradiation effects on materials (Nordlund 2019). In UO_2, it has been

shown that interstitial dislocation loops appear spontaneously after irradiation-induced displacement cascades due to a loop-punching process (Van Brutzel et al. 2008; Martin et al. 2010). Martin *et al.* have identified subnanometric faulted {111} prismatic loops evolving into the same unfaulted {110} loop than those observed by Le Prioux *et al.* as the loop diameter increases during irradiation simulation (Martin et al. 2010). This unfaulting mechanism involves a Shockley partial dislocation as described in the work of Chartier *et al.* (Chartier et al. 2016). Overall, these studies confirm the higher stability of the unfaulted {110} prismatic loop when the loop diameter exceed the nanometer, as observed in aforementioned TEM experiments.

While individual primary 1/2<110>{001} dislocations and irradiation-induced {110} loops were widely characterised in recent years, very little is known about their interactions and how the latter may impact the fuel pellet mechanical behaviour at low-to-intermediate dose and, consequently, the cladding mechanical integrity during accidental conditions. In the present work, we use MD and DDD to investigate for the first time the interactions between 1/2<110>{001} glissile dislocations and {110} irradiation prismatic loops in UO_2 under accidental operating conditions, and quantify their contribution to hardening. We first characterise the possible contact reactions between individual primary dislocations and prismatic loops using MD at 2000 K as function of their relative orientation. A particular attention is paid to the various mechanisms (cross-slip, junction formation, *etc.*) involved during the reactions. To allow for an upscaling, each reaction characterised using MD is reproduced using DDD, confronting the elastic theory to atomic-scale observations. Finally, DDD is used to simulate the behaviour of 1/2<110>{001} primary dislocations gliding through a population of {110} irradiation loops typical of experiments and model the strengthening induced by the collective behaviour of irradiation dislocation loops. This study makes it possible to outline irradiation hardening in the main nuclear fuel for the first time via a multi-scale modelling approach.

2. Simulation methods

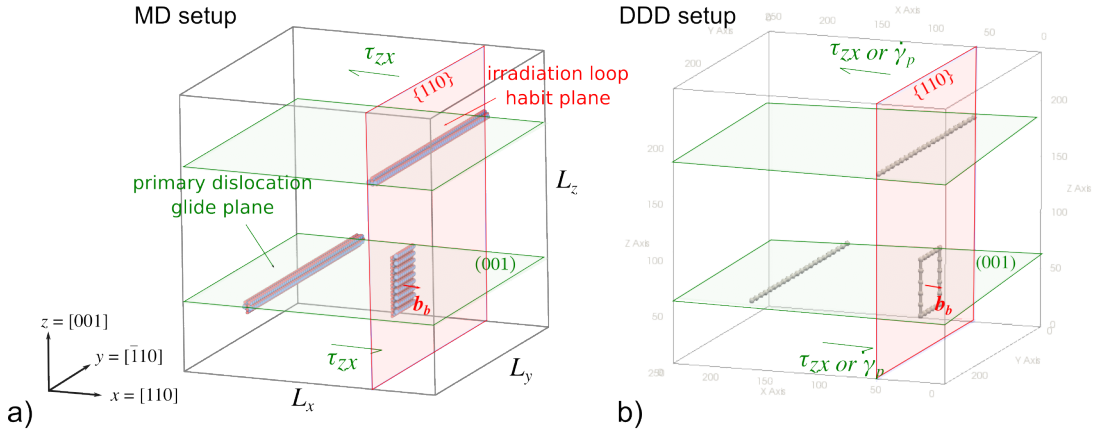

Figure 1: Simulation protocol to study the local interaction between a glissile dislocation and a single irradiation loop using a) MD and b) DDD. The glissile dislocation line is oriented along $\boldsymbol{y}$=[$\bar{1}$10], perpendicularly to the slip plane normal $\boldsymbol{z}$=[001]. The Burgers vector is along $\boldsymbol{x}$ or $\boldsymbol{y}$ depending on the dislocation character (edge or screw, respectively). The {110} habit plane of the irradiation loop and its Burgers vector $\boldsymbol{b_b}$ are oriented along $\boldsymbol{x}$ in the figure but the $\boldsymbol{y}$ and [011] orientations are also investigated. The same simulation cell length L_x=24.4 nm, L_y=24.6 nm and L_z=23.9 nm is used for both simulation methods. U and O defect atoms in MD are coloured in blue and red respectively (perfect crystal atoms are removed for the sake of clarity) while dislocation lines and nodes are coloured in light-grey in the DDD subfigure. Primary dislocation glide plane and irradiation loop habit plane are coloured in green and red, respectively.

Here we use atomistic and DDD simulations to investigate dislocation *vs.* prismatic loop interactions and the resulting hardening in UO_2 under accidental operating conditions. MD simulations are performed using the Large-scale Atomic/Molecular Massively Parallel Simulator (LAMMPS) (Thompson et al. 2022) and the rigid-ion potential

adjusted by Potashnikov *et al.* (Potashnikov et al. 2011). This potential was recently successfully used to model dislocation core and mobility in UO_2 (Lunev et al. 2017; Lunev et al. 2018; Borde et al. 2022). Following the previous work of Borde *et al.* (Borde et al. 2022), the Wolf truncation method is used to handle coulombic interactions with the Wolf radius and damping coefficient set to 11 Å and 0.3 $Å^{-1}$, respectively. Short-range interactions are also cut-off at 11 Å. Atomic configurations are characterised using Ovito (Stukowski 2009) and the polyhedral template matching (PTM) crystallography algorithm (Larsen et al. 2016) applied to the uranium face-centered cubic (FCC) sublattice.

In MD simulations, glissile dislocations are modelled using the dislocation dipole method (Cai et al. 2003; Rodney et al. 2017) to build neutral dislocation cores in UO_2 without charge excess in a 3D-periodic simulation cell, see discussion in (Borde et al. 2022). Both edge and screw dipole configurations are modelled using a simulation cell oriented along $\boldsymbol{x}$=[110], $\boldsymbol{y}$=[$\bar{1}$10] and $\boldsymbol{z}$=[001] that is sufficiently large (L_x=24.4 nm, L_y=24.6 nm and L_z=23.9 nm) to avoid dislocation interactions within the dipole and with periodic replica. The dislocation-loop interaction simulation follows a well-established protocol inspired by what is usually done in metals (Rodney 2004; Bacon et al. 2009; Arsenlis et al. 2012; Erel et al. 2017). As shown in Figure 1a, a stoichiometric and unfaulted {110} interstitial loop typical of UO_2 (see Le Prioux et al. 2016 and aforementioned TEM literature) is inserted in the simulation cell in front of one of the glissile dislocations. For that purpose, a temporary-free space is first generated at the location of the loop by displacing the atoms apart using the Barnett formulation of displacement fields (Barnett 1985) as implemented in ATOMSK (Hirel 2015). Then, a square-shaped loop of edge length l_b made of two <110>-oriented crystalline planes is inserted filling the empty space. As in the work of Le Prioux *et al.,* the square prismatic loop is made of two pairs of parallel edge dislocations of same Burgers vector $\boldsymbol{b_b}$=1/2<110> lying in {001} and {110} crystallographic planes, respectively. The square shape of the extended defect is neutral-charged, which guarantees to preserve the stoichiometry of the sample. Prismatic loop with l_b ranging from 3 to 8 nm were considered as observed in experiments, with a special focus on l_b=5 nm. After constructing the initial configuration, the internal energy of the system is minimised allowing for the full simulation cell relaxation *i.e.*, the six terms of the global stress tensor have a zero pressure target, using molecular statics and a force norm criterion of 10^{-10} eV/Å. Then, the system is heated up to 2000 K (temperature typical of the accidental operation regime) at a heating rate $\dot{T}$=50 K/ps using MD and the Nosé-Hoover thermostat in the NPT ensemble before running an additional 10 ps equilibration at constant temperature. A timestep δt=1 fs is used for all MD simulations in the study. Contact reactions between glissile dislocations and prismatic loops are investigated at T=2000 K under an applied shear stress τ=900 MPa. The stress component of interest (τ_{zx} for the edge dislocation and τ_{zy} for the screw dislocation) is monitored using the Nosé-Hoover barostat while the other components are maintained at zero.

DDD simulations are performed using the parallel nodal code Numodis that was recently used to investigate the influence of irradiation-induced defects in metals such as iron and zirconium alloys with one-to-one comparison to MD simulations (Drouet et al. 2014; Shi et al. 2015; Li et al. 2019). From a technical point of view, Numodis is a C++ nodal DDD code, in which dislocations are described using nodes interconnected by segments characterised by their Burgers vector and glide plane. In this study, the force acting on a node is computed using the non-singular dislocation theory (Cai et al. 2006) with a core-width equal to the Burgers vector amplitude b and the analytical formulation derived by Arsenlis *et al.* (Arsenlis et al. 2007). A lattice parameter a_0=5.43 Å is used as well isotropic elastic properties ν=0.3 and μ=74 GPa, close to experimental 2000 K conditions (Jackson et al. 1986).
The velocity of each node is computed using a classical variational approach (Weygand et al. 2002; Cai et al. 2006) and dislocation segments are displaced according to an overdamped equation of motion, $v(\tau) = \tau.b/B_i$, with B_i the damping coefficient used to describe dislocation glide in slip mode i in the athermal regime of deformation. Here we use B_I=2.2 10^{-3} Pa.s for the 1/2<110>{001} glissile dislocations as well as for the prismatic loop edge segments lying in {001} planes. This value is derived from MD simulations of 1/2<110>{001} dislocation mobility using the same Potashnikov potential and performed in the same temperature range (Borde et al. 2022). In the absence of quantitative data about the 1/2<110>{110} edge dislocation mobility in UO_2, B_{II} was artificially set four times larger for the prismatic loop edge segments in {110} planes (B_{II}=8.8 10^{-3} Pa.s) scaling with the larger CRSS values measured for the deformation mode II at 2000 K (Nadeau 1969; Fossati et al. 2013; Portelette et al. 2018). Dislocation contact reactions (junction, annihilation, crossed-states, *etc.*) in Numodis are computed using the elastic theory, allowing to model dislocation microstructure evolution and strain hardening. As inspired from the work of Bulatov and collaborators (Bulatov and Cai 2006; Arsenlis et al. 2007), a collision detection algorithm is used to predict

incoming dislocation contact reactions. Also, a cross-slip criterion for the screw dislocation is used to model cross-slip from 1/2<110>{001} to either 1/2<110>{110} or 1/2<110>{111} slip systems, as observed in UO_2 experiments at temperatures beyond 1600 K (Yust and McHargue 1969; Sawbridge and Sykes 1971). Note that cross-slip is not always activated in the following simulations and its use will be explicitly mentioned. The cross-slip model relies on a simplified approach of the Friedel-Escaig model as developed by Kubin for FCC metals (Kubin 2013), and adapted to the fluorite crystallography for which several slip modes have to be considered. Indeed, here the shear stress in the cross-slip system τ_{css} is directly compared to stress in the primary slip system τ_s after the screw segment identification (θ<2°, with θ the angle between $\boldsymbol{b}$ and the line vector $\boldsymbol{l}$), instead of using the FCC stage III stress. Probable cross-slip system (css) geometries are provided as simulation inputs. From there, if $\tau_{css}>\tau_s/tol$ at a dislocation node (with tol a tolerance factor), one computes the cumulative screw length l_s for which the previous condition is verified and the cross-slip probabilities in all the possible css are computed as,

$$P(l_s, \tau_{css}) = \frac{l_s}{l_0}\frac{\delta t}{\delta t_0} A e^{-\frac{\Delta H_0}{k_b T}} e^{\frac{V(|\tau_{css}|-\tau_s)}{k_B T}} \tag{1}$$

where l_0=1 µm and δt_0=1 ns are characteristic length and time in the range of the DDD discretization space, δt=1 fs is the DDD timestep (equivalent to the MD one to allow self-comparison), k_bT is the Boltzmann factor and A=7500 is a scaling prefactor. Cross-slip activation parameters ΔH_0=2.8 eV and V=250 nm^3 as well as tol=0.9 are set to mimic parts of MD observations, they will be further discussed in the following.

Two setups are used for the DDD simulations. Firstly, local interactions between individual glissile dislocations and prismatic loops are investigated in the same conditions as in MD (Figure 1). This allows to check the parameters introduced in Numodis (*e.g.,* mobility, cross-slip parameters) and verify the application of the isotropic elastic theory to dislocation-irradiation loop interactions in UO_2. To be as close as possible to the MD conditions, DDD is performed using periodic boundary conditions (PBCs) with the same simulation cell dimensions, timestep and shear stress conditions. Also, the dislocation dipole and irradiation loop are inserted at exact same locations as in the MD simulation. Besides mimicking the MD simulation, the DDD-MD self-similar setup is used to run a parametric study focusing on the influence of the applied shear stress on the dislocation *vs.* prismatic loop interaction. Secondly, statistical DDD simulations are performed to investigate the hardening induced by a large number of {110} prismatic loops (Figure 2). For that purpose, an extended simulation volume of 200×200×50 nm^3 size and a single glissile edge or screw dislocation are used, as illustrated in Figure 2. Here, PBCs are used in the dislocation glide plane while free-BCs are applied in the z-direction normal to the glide plane. A density of square-shaped irradiation loops ρ_b=10^{22} m^{-3} is simulated, corresponding to densities measured experimentally (Onofri et al. 2016). For this second setup, a constant shear rate $\dot{\gamma}$=10^5 s^{-1} corresponding to an averaged dislocation velocity of 2.5 m.s^{-1} is used. DDD simulations are analysed using the Paraview software (Henderson et al. 2004).

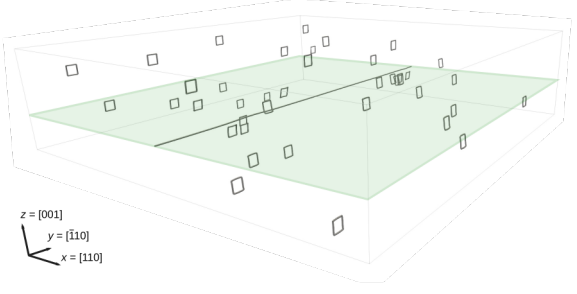

Figure 2: Statistical dislocation-prismatic loop DDD simulation at constant shear rate. The simulation cell contains a glissile {001} dislocation located at the centre of the box and a population of {110} irradiation loops with a density ρ_b=10^{22} m^{-3}.

3. Simulation results

Due to symmetries, six dislocation-loop configurations (3 for the primary edge dislocation, 3 for the screw) labelled cases #1 to #6 need to be investigated. The six configurations are described in Figure 3 and summarised in Table 1. The angle β formed by the Burgers vectors of the glissile dislocation and the prismatic loop ($\boldsymbol{b_d}$ and $\boldsymbol{b_b}$, respectively) is either 0° (parallel Burgers vectors, cases #1 and #4 for the edge and screw dislocations respectively), 90° (perpendicular Burgers vectors, cases #2 and #5) or 120° (cases #3 and #6). In the following, glissile dislocation *vs.* prismatic loop reactions are rationalised in terms of hardening-induced intensity, namely weak, intermediate and strong interactions. The classification proposed by Bacon *et al.* (Bacon et al. 2009; Osetsky and Bacon 2012) is used to summarise the different reaction products as shown in Table 1:

- R1: the obstacle and dislocation remain unchanged;
- R2 : the obstacle is modified by the interaction, but the dislocation remains unchanged;
- R3: the obstacle is partially or entirely absorbed by the dislocation in the form of a superjog;
- R4 : the obstacle is temporarily absorbed on the screw dislocation in the form of a helical turn.

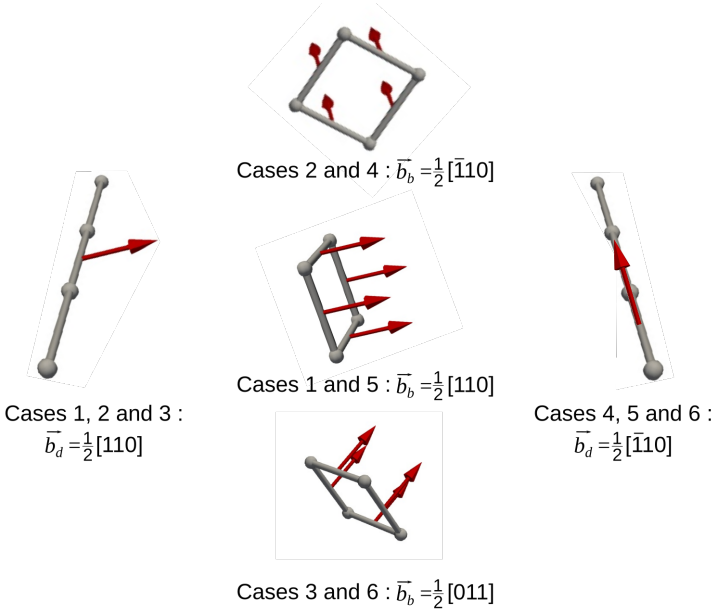

Figure 3: Dislocation-prismatic loop configurations as function of the Burgers vectors (red arrows) relative orientation. Due to symmetries, the (001) edge with $\boldsymbol{b_d}$=1/2[110] and the screw dislocation with $\boldsymbol{b_d}$=1/2[$\bar{1}$10] are studied interacting with three {110} prismatic loops characterised by $\boldsymbol{b_b}$=1/2[110], 1/2[$\bar{1}$10] and 1/2[011], respectively.

3.1. Weak hardening

The first case considered is case #2, characterised by the interaction between a 1/2[110] edge dislocation and a prismatic loop with a perpendicular Burgers vector (β=90°), see Figure 4. The glissile dislocation line direction and the Burgers vector of the prismatic loop are both oriented along [$\bar{1}$10]. For $l_b \geq$5 nm in the MD and DDD simulations, the mobile dislocation goes through the prismatic loop without notable attraction or repulsion, as expected from the elastic theory in the case of dislocations with orthogonal Burgers vectors. Furthermore, no clear contact reaction is observed. Indeed, using the Frank criterion $b_j^2=b_d^2+b_b^2$ (with b_j the Burgers vector length of the junction that could possibly form) and since β=90°, we observe that the Hirth$_{I/II}$ junction that could result from the interaction between a 1/2<110>{001} glissile dislocation and a {110} prismatic loop segment with orthogonal Burgers vectors is only marginally stable, as discussed in the work of Portelette *et al.* who considered dislocation-forest interactions in UO_2 using DDD (Portelette et al. 2020). In this work, the authors showed that the Hirth$_{I/II}$ junction formation probability is low and often leads to a crossed state (attractive configuration without junction formation). The corresponding hardening coefficient obtained

Table 1
{001} dislocation *vs.* {110} irradiation loop reaction table in UO_2. β is the the angle between the two Burgers vectors. R1 to R4 refer to Bacon *et al.* classification (Bacon et al. 2009; Osetsky and Bacon 2012).

Dislo. character	Case	β	Hardening	Bacon class.
edge	#1	0°	intermediate	R3
	#2	90°	weak	R1
	#3	120°	intermediate	R3
screw	#4	0°	strong	R4
	#5	90°	intermediate	R1
	#6	120°	strong	R4

by Portelette *et al.* is particularly low ($\alpha_6 = 0.09$). Therefore, case #2 should only have a limited contribution to irradiation-hardening in UO_2 by analogy. This reaction is of R1 type according to Bacon *et al.* classification. Finally, one can note that point defects are emitted during the reaction in the MD simulation, confirming previous observations (Lunev et al. 2017; Soulié et al. 2018).

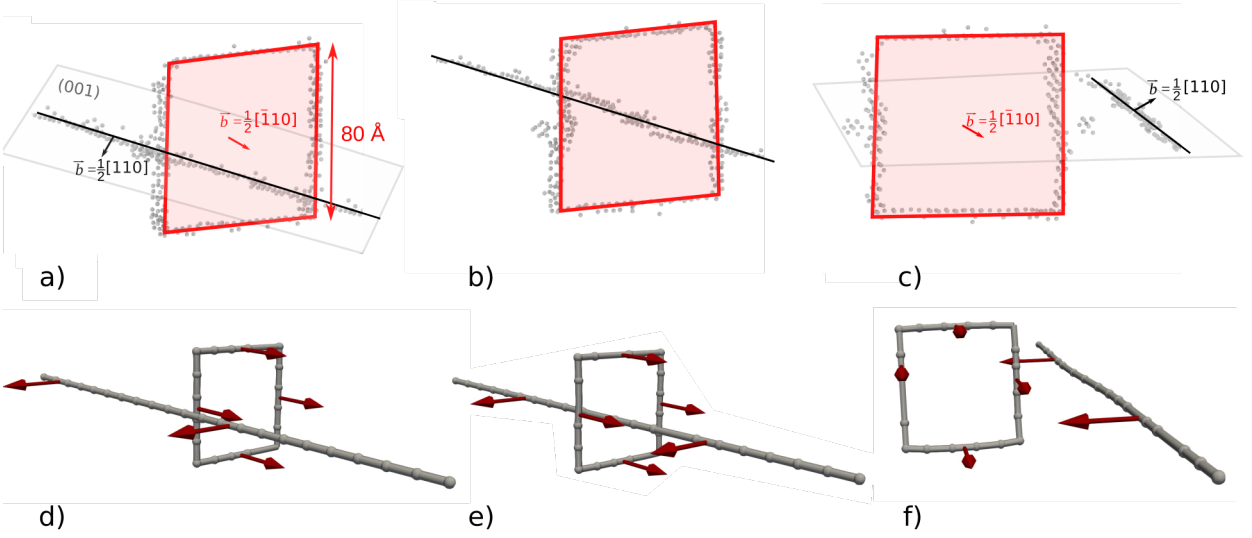

Figure 4: Interaction between a 1/2[110](001) edge dislocation and a 1/2[$\bar{1}$10]($\bar{1}$10) prismatic loop (case #2, β=90°, l_b=80 Å). (a-c) MD simulation. Dislocation atoms identified using the PTM algorithm are shown in grey. Lines and arrows show dislocation lines and Burgers vectors (black: glissile dislocation, red: irradiation loop), (d-f) DDD simulation. Dislocation lines and Burgers vectors are coloured in grey and red, respectively.

A constant shear rate DDD simulation with the same 1/2[110](001) edge dislocation gliding through a population of 1/2[$\bar{1}$10]($\bar{1}$10) prismatic loops (l_b=5 nm, ρ_b=10^{22} m^{-3}) is illustrated in Figure 5. The simulation shows that the dislocation is only weakly impacted by the prismatic loops, as expected from the local interaction simulations described above. The glissile dislocation interacts with the loop vertical segments leading to Hirth junctions that break easily. Also, one can notice interactions with the horizontal segments of the prismatic loops that pin the edge dislocation (Figure 5a). As shown in Figure 5b, these interactions slightly influence the mechanical response that becomes jerky with a maximum stress increase of about 30 MPa, typical of a weak hardening.

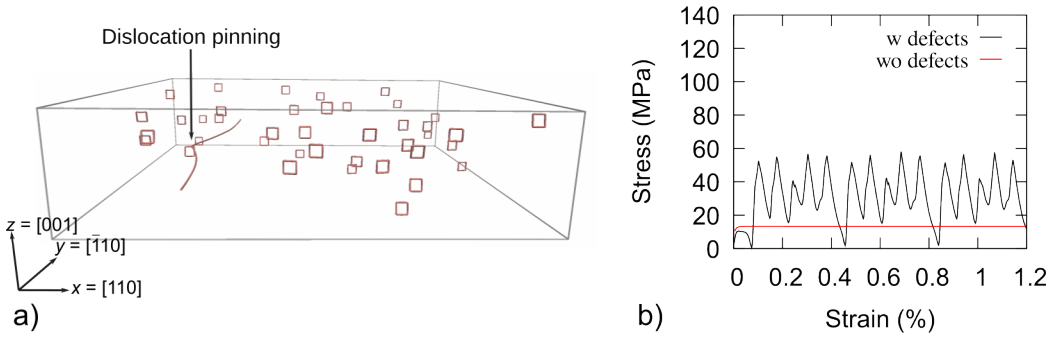

Figure 5: DDD simulation at constant shear rate of a 1/2[110](001) edge dislocation gliding through a population of 1/2[1̄10](1̄10) prismatic loops (case #2, l_b=5 nm, ρ_b=10^{22} m^{-3}). (a) Illustration of the pinning process of the glissile dislocation by a prismatic loop. (b) Stress-strain curves with (black) and without (red) irradiation defects.

The dispersed barrier hardening (DBH) model (Seeger 1958) allows to express the hardening due to randomly localised obstacles as a function of their density and size with the following relationship,

$$\Delta\tau = \alpha\mu b_d\sqrt{Nd} \tag{2}$$

where $\Delta\tau = <\tau> - \tau_0$ is the shear stress increase induced by the population of defect obstacles, $<\tau>$ and τ_0 being the shear stress with and without defects respectively (see *e.g.,* Figure 5b), α the hardening coefficient, N=ρ_b the irradiation loop density and d is the average loop diameter (here $d = l_b$). The flow stress in presence of irradiation loops $<\tau>$ is calculated as the average of the stress peaks that is the relevant obstacle strength measure (Rodney and Proville 2009). A square-root dependence with a hardening coefficient α=0.06, slightly lower than the hardening coefficient obtained for the $Hirth_{I/II}$ junction (α_6=0.09±0.02) by Portelette *et al.* (Portelette et al. 2020), is observed when plotting the stress increase measured in the DDD simulations as a function of the loop density ρ_b (Figure 6). This result confirms that the interaction of 1/2<110>{001} edge dislocations with {110} irradiation loops with an orthogonal Burgers vector generates only weak hardening.

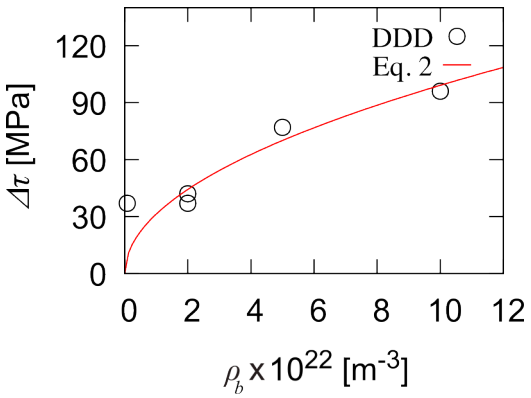

Figure 6: Strengthening $\Delta\tau$ *vs.* irradiation loop dislocation density ρ_b (case #2, β=90°, l_b=50 Å). DDD results and Equation 2 model are shown using black symbols and a red curve, respectively.

3.2. Intermediate hardening

We now consider cases #1, #3 and #5 that produce an intermediate hardening. Cases #1 and #3 correspond to a glissile edge dislocation with β=0° and 120°, respectively. Figure 7a-c illustrates the local contact reaction for case

#1 as simulated by MD. Here, the mobile dislocation and the loop have the same 1/2[110] Burgers vector. When the dislocation comes into contact with the side segments of the loop (Figure 7a), collinear reactions (Madec et al. 2003) occur on both sides, leading to exchanges between the dislocation arms and the loop segments (Figure 7b). As a result, the mobile dislocation absorbs the upper part of the loop while its lower part remains below the dislocation glide plane. In the process, the loop is cut in half and the dislocation acquires two superjogs that can be dragged away (Figure 7c) since, for an edge dislocation, the Burgers vector is in the glide direction. This R3 interaction mechanism according to Bacon *et al.* classification was observed for l_b=30 and 50 Å and is perfectly reproduced using DDD (Figure 7d-f). Since the superjogs can be dragged by the edge dislocation in its motion, case #1 does not show a strong static pinning but only a drag effect *i.e.*, a rate-dependent slowdown of the edge dislocation due to the reduced mobility of the superjogs. The present collinear reaction is different from the forest $collinear^{90\text{-}}_{I/II}$ reaction studied by Portelette *et al.* in case of interacting mode I and II dislocations with same Burgers vectors (Portelette et al. 2020). The latter is characterised by significant portions of the dislocations that annihilate leading to a strong static pinning and a significant hardening coefficient (α_5=0.81±0.05). Case #3 with β=120° will not be further discussed as it leads to the same formation of superjogs on the 1/2<100>{001} edge dislocation with similar implications for irradiation hardening.

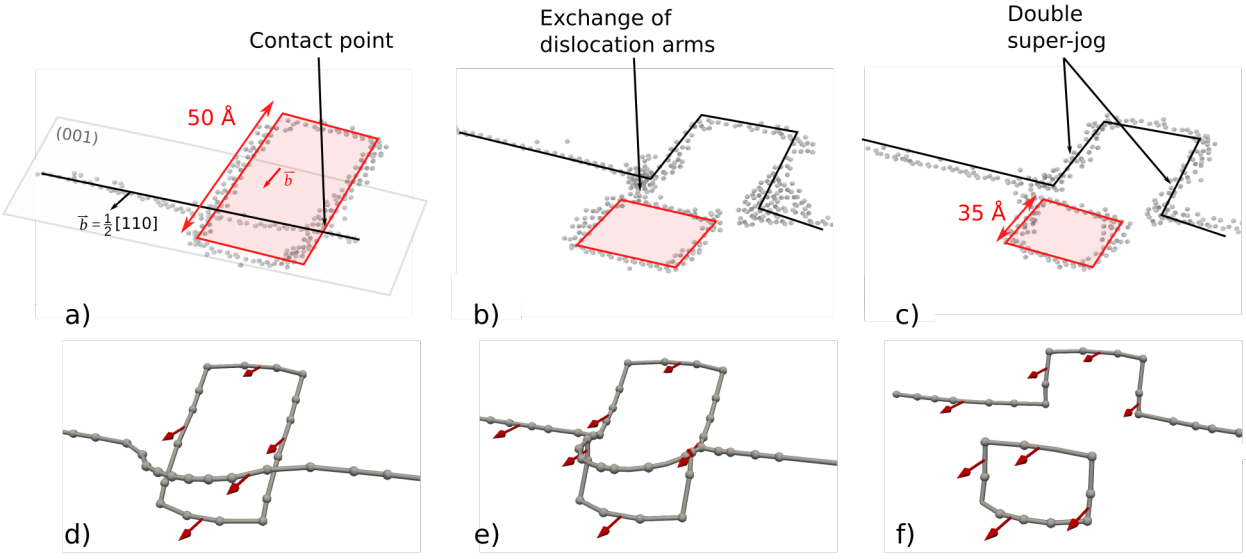

Figure 7: Interaction between a 1/2[110](001) edge dislocation and a 1/2[110](110) prismatic loop (case #1, β=0°, l_b=50 Å). (a-c) MD simulation. (d-f) DDD simulation. The same symbols and colour code are used as in Figure 4.

Case #5 in Figure 8 shows the interaction between a screw dislocation and an irradiation loop with perpendicular Burgers vectors (β=90°). The MD simulation shows that once the screw dislocation comes close to the prismatic loop (Figure 8a), it cross-slips in the $(11\bar{1})$ plane towards the bottom edge of the loop and creates a Hirth coplanar junction with $\boldsymbol{b}_j=[0\bar{1}0]$ (Figure 8b). Except in the case of interfaces (Liu et al. 2011), coplanar junctions are rarely discussed in the literature due to the low probability of having two dislocations in the exact same crystallographic plane. However, the dislocation-prismatic loop interaction configuration at high-temperature is a system where this situation happens more frequently due to the proximity of dislocation segments that can interact via thermally-activated cross-slip. Here, the freshly-formed junction is marginally stable and quickly breaks, releasing the screw dislocation (Figure 8c) and resulting in a R1 mechanism. This behaviour is reproduced in the DDD simulation when cross-slip is activated (Figure 8d-f). If not, the glissile dislocation shears the prismatic loop without contact reaction as expected by the elastic theory when β=90° (same as case #2, Figure 4) and continues to glide (Figure 8g-i). Finally, DDD shows that the screw dislocation mobility is only weakly impacted by the irradiation loop (β=90°), regardless of cross-slip.

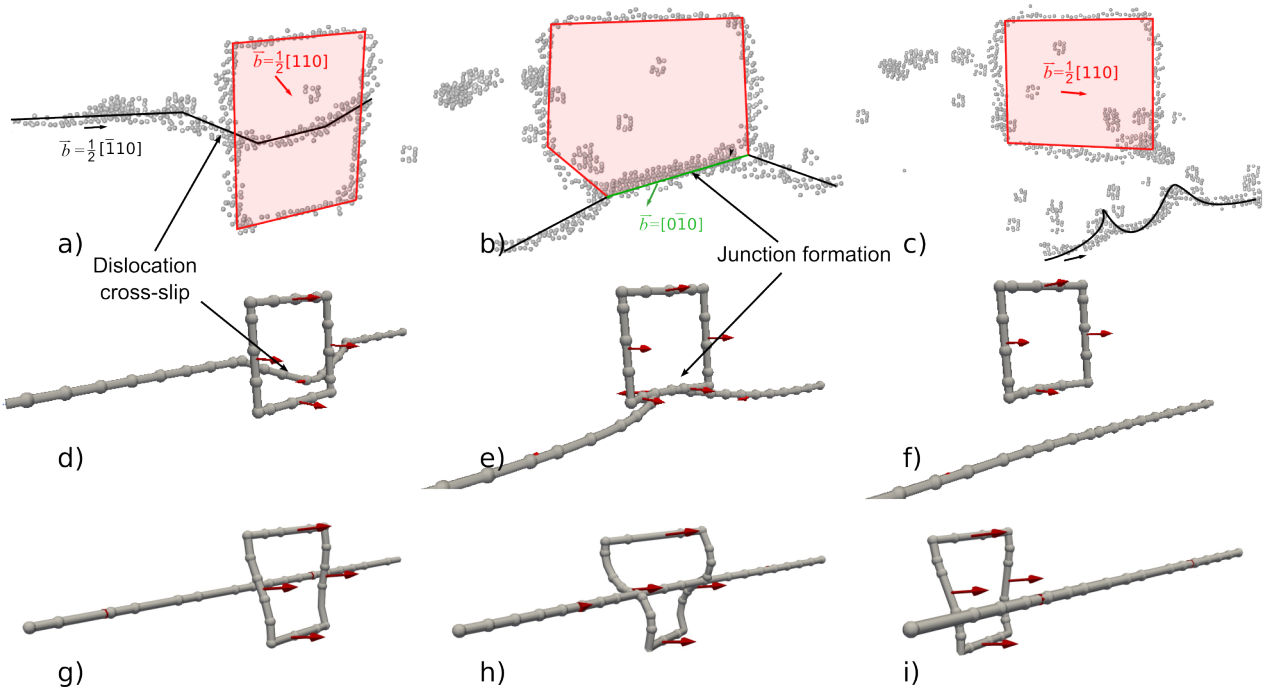

Figure 8: Interaction between a 1/2[$\bar{1}$10](001) screw dislocation and a 1/2[110](110) prismatic loop (case #5, β=90°, l_b=50 Å). (a-c) MD simulation. (d-f) DDD simulation with cross-slip. (g-i) DDD simulation with cross-slip turned off. The same symbols and colour code are used as in Figure 4.

Turning to the large-scale DDD simulations at constant shear rate, cases #1 and #5 show some similarities. When the dislocation gets close to an irradiation loop, the latter pairs with the glissile dislocation and is pushed forward in the $\boldsymbol{b_b}$ direction due to the dislocation stress field. One can note that this mechanism operates without contact reaction *i.e.,* the reactions described in Figures 7 and 8 are not observed in constant shear rate DDD simulations performed under lower stress conditions. This process repeats each time the dislocation meets a prismatic loop, leading to the formation of a cloud of irradiation defects surrounding the glissile dislocation. This process is illustrated in Figure 9a. Despite the cloud formation, the dislocation continues to glide, dragging along the neighbouring defects (*drag effect*) and clearing an entire domain within the sample. The latter leads to the formation of a clear band, a well-known process generally observed in metals under irradiation (Sharp 1967; Robach et al. 2003; Nogaret et al. 2008).

Figure 9b shows the corresponding stress-strain curves. The stress increases at the beginning of the simulation as more prismatic loops pair with the mobile dislocation *i.e.,* the prismatic loop cloud formation slows down the dislocation. After the dislocation has travelled slightly more than one simulation cell pass (~0.4% strain), the stress reaches a steady-state plateau (*c.a.,*75 MPa for case #5, 110 MPa for case #1) that corresponds to the cloud saturation and the formation of the clear band. The DBH model (Equation 2) can not be applied for cases #1, #3 and #5 due to the lack of contact reactions and the dynamic aspect of the corresponding strain hardening. Overall, these cases are examples of intermediate hardening induced by irradiation loops in UO_2 in the relatively high strain rate conditions imposed in the DDD simulation. This later aspect will be further detailed in the discussion.

3.3. Strong hardening

The only cases of strong pinning are cases #4 and #6, which correspond to the interaction between a screw dislocation and irradiation loops with parallel or 120° Burgers vectors (β=0° or 120°), respectively. Such a typical contact reaction is illustrated in Figure 10 where a splitting process happens *i.e.,* a collinear reaction with an arm exchange, when the mobile dislocation comes into contact with the loop. Thus, the loop opens like a sheet of paper being torn, along the dislocation line direction [$\bar{1}$10] and the loop is absorbed in the form of a helical turn on the screw dislocation. This kind of reaction is ranked R4 according to Bacon *et al.*. As a consequence, the dislocation motion is stopped as, in

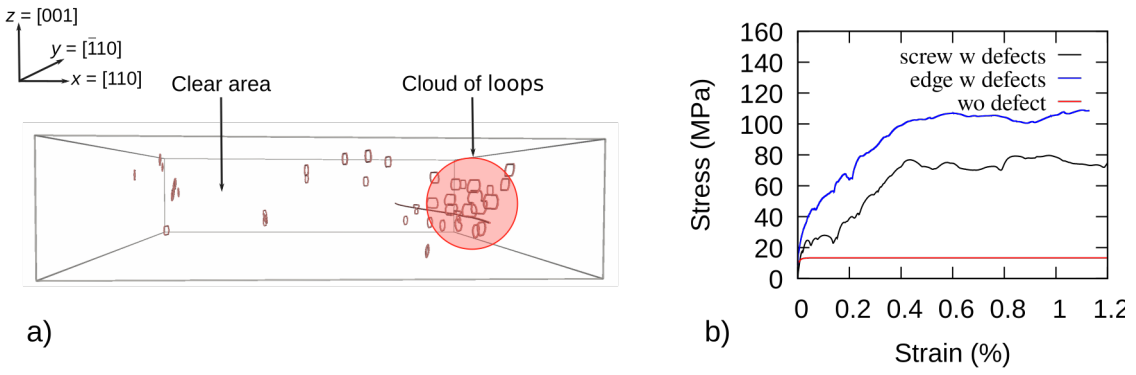

Figure 9: DDD simulation at constant shear rate of a dislocation gliding through a population of 1/2[110](110) prismatic loops (cases #1 and #5, l_b=5 nm, ρ_b=10^{22} m^{-3}). (a) Illustration of the drag effect characterised by the formation of a cloud of prismatic loops (red halo) that surrounds the glissile dislocation at the root of clear band formation (case #5). (b) Stress-strain curves obtained for case #1 (blue), case #5 (black) and without irradiation defects (red).

contrast with cases #1 and #3, a helical turn can not be dragged since it can only move along the dislocation Burgers direction and not along its glide direction, leading to a strong pinning configuration. Rodney *et al.* have observed the same helical configuration in FCC metals and have shown that the mobile dislocation can bypass the helical turn via an Orowan process, which forces the helical turn to close onto itself to reconstruct the initial loop (Rodney 2004). This was also observed here for a dislocation length of ∼150 nm using DDD.

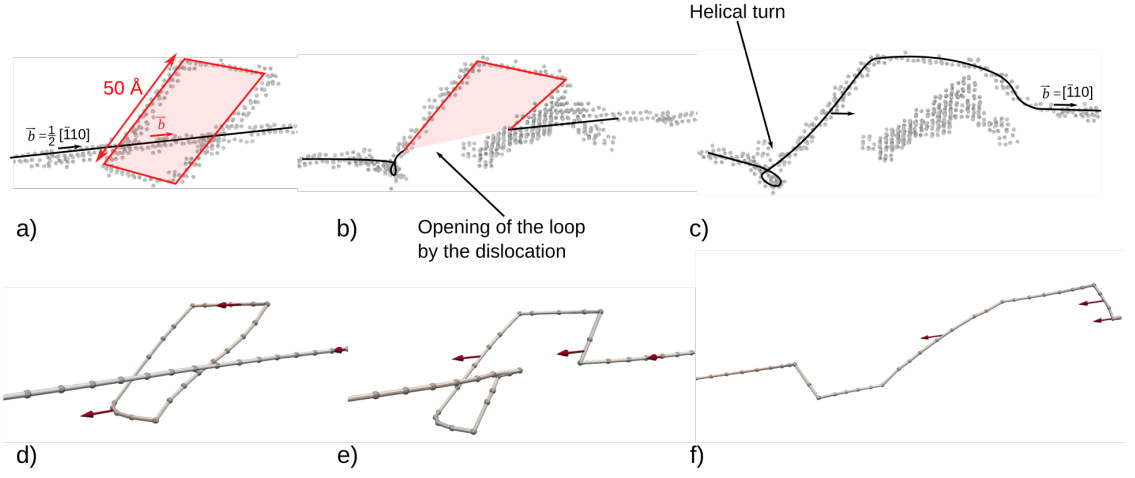

Figure 10: Interaction between a 1/2[$\bar{1}$10](001) screw dislocation and a 1/2[$\bar{1}$10]($\bar{1}$10) prismatic loop (case #4, β=0°, l_b=50 Å) leading to the formation of a helical turn. (a-c) MD simulation. (d-f) DDD simulation. The same symbols and colour code are used as in Figure 4.

Figure 11 shows a large-scale DDD simulation for case #4. At the beginning of the simulation, the dislocation glides under a moderate stress, but quickly gets strongly pinned by the formation of helical turns. The stress increases considerably, reaching a critical value of about 1 GPa before unpinning (Figure 11b). This result confirms the strong hardening effect of helical turns. The stress will vary further depending on the geometry of the encountered defects *e.g.,* the first stress peak observed in Figure 11b is related to the formation of two helical turns close to each other while the next peaks at lower stresses starting near 0.8% strain correspond to successive pinning/unpinning sequences

from single helical turns. Unpinning proceeds by moving the helical turns along the line to generate long enough screw segments to undergo Orowan processes around the loops. In doing so, the loops are pushed to the sides, clearing a region around the dislocation glide plane. This *shovelling* effect leads to the formation of a clear band as already observed in cases #1 and #5.

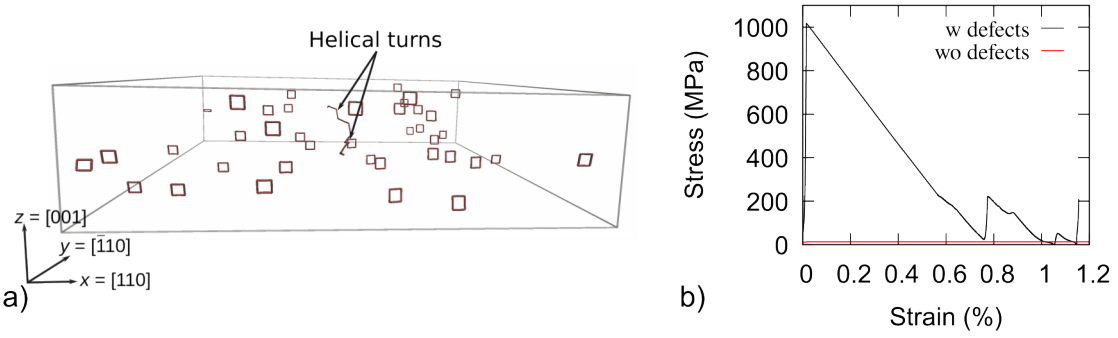

Figure 11: DDD simulation at constant shear rate of a screw dislocation gliding through a population of 1/2[$\bar{1}$10]($\bar{1}$10) prismatic loops (case #4, l_b=5 nm, ρ_b=10^{22} m^{-3}). (a) Formation of helical turns along the dislocation line. (b) Stress-strain curves with (black) and without (red) irradiation defects.

4. Discussion

Hardening caused by dislocation *vs.* irradiation defect interactions has been widely studied in the literature, particularly in metals. Among others, Osetsky *et al.* have investigated dislocation-loop and dislocation-stacking fault tetrahedron (SFT) interactions using MD (Osetsky et al. 2006; Bacon et al. 2009). DDD was used to study grain-scale plastic flow, modelling elementary dislocation-loop interactions in FCC metals (Zbib et al. 2000; Ghoniem et al. 2001; Nogaret et al. 2008). Arsenlis *et al.* have used DDD to better understand the embrittlement and hardening of irradiated iron, accounting for detailed dislocation-loop interactions (Arsenlis et al. 2012) and Cui *et al.* used DDD/FEM coupling to apply barrier field models to irradiated materials (Cui et al. 2018). Also, Rodney (Rodney 2004; Nogaret et al. 2008) and Baudouin *et al.* (Baudouin et al. 2015) have used MD to study the interaction between glissile dislocations and Frank loops in Ni and Cu and a FeNiCr alloy, respectively. In the same way, Drouet *et al.* (Drouet et al. 2014) studied the interactions between dislocations and irradiation loops in zirconium using DDD. Finally, Shi *et al.* (Shi et al. 2015) focused on dislocation-irradiation loop interactions using both MD and DDD in high-temperature ferrite. The authors also investigated the role of a population of irradiation loops using MD. However, none of such approaches was applied to irradiation in UO_2 up to now. With regards to the literature, the helical configuration observed in cases #4 and #6 is a classic case when a screw dislocation interacts with a prismatic loop with same Burgers vector, or when a faulted loop or a SFT reacts with the screw dislocation, leading systematically to significant hardening (Rodney 2004; Bacon et al. 2009; Drouet et al. 2014; Shi et al. 2015; Erel et al. 2017). The dislocation arm exchange and superjog formation observed in case #1 (edge, β=0°) have also been observed in metals (Rodney and Martin 1999; Bacon et al. 2009; Drouet et al. 2014; Baudouin et al. 2015). Various aspects related to stress amplitude, size effect, clear band formation and the corresponding interaction mechanisms and hardening are discussed in the following.

Influence of stress

In the present study, local interaction simulations between individual dislocations and prismatic loops were performed at an elevated applied stress (*c.a.,* 900 MPa) when compared to stresses measured in experiments. This is due to the reduced timescale imposed by the MD method. However, one can take advantage of the DDD technique to decrease the stress level and the dislocation velocity as done in the DDD simulations at constant shear rate. Varying the shear rate allows to verify the influence of the stress amplitude on the dislocation-loop interactions and check the transferability of high-stress MD simulations to experimental conditions of deformation. Thus, additional DDD simulations were

performed at shear rates ranging from $\dot{\gamma}_p$=10^5 to 7 10^6 s^{-1}, corresponding to a flow stress between 10 to 900 MPa, depending on the investigated case. Although some interactions show no sensitivity to the shear stress (*e.g.,* cases #4 and #5), others (case #1) exhibit significant differences. For $\dot{\gamma}_p$ >10^6 s^{-1} (equivalent to $<\tau>$ larger than 60 MPa), the arm exchange occurring in case #1 (edge dislocation, β=0°) is exactly the same as seen in Figure 7. However, at $\dot{\gamma}_p$ = 10^6 s^{-1} ($<\tau>$∼60 MPa), the prismatic loop starts to glide as the dislocation approaches, due to the repulsive stress gradient induced by the latter. At this shear rate, the dislocation catches up with the loop that has a lower mobility due to the slower mode II segments. However, lowering further the shear rate down to 10^5 s^{-1} ($<\tau>$∼10 MPa) amplifies this effect *i.e.,* the loop is pushed by the dislocation and the contact reaction no longer occurs. So, while the elastic interaction between the dislocation and the prismatic loop is repulsive, the dislocation contacts with the prismatic loop only if its mobility (and thus, the shear stress) is large enough for the dislocation to catch up with the loop. Otherwise, the loops are simply dragged as observed in the large-scale DDD simulation of Figure 9. We thus observe a sensitivity to the defects relative mobility in the DDD simulation that is not captured by high-stress MD simulations. While only statistical massive simulations would be able to quantify the influence of this relative-mobility effect on strain hardening, the repelled prismatic loops might still be stopped by local stress-field variations induced by neighbouring defects, leading back to contact reactions. Also, this phenomenon relies strongly on the prismatic loop mobility that requires more investigations, especially for mode II edge dislocation segments that have not yet been studied in the literature. In a lesser extent, case #2 (edge dislocation, β=90°), which originally showed no reaction, also exhibits some stress sensitivity. Indeed, the formation of a junction is observed when the mobile dislocation intersects the prismatic loop if the shear rate is lowered down to 1.2 10^6 s^{-1} ($<\tau>$∼150 MPa) . However, the resulting $Hirth_{I/II}$ junction is only marginally stable and should not play a significant role in irradiation hardening.

Size effect

For the larger prismatic loops investigated here (l_b>5 nm), we generally did not observe any size effect, whatever the case studied. However, case #2 (edge dislocation, β=90°), that originally did not lead to contact reactions in the MD simulation (see Figure 4), has shown a particular behaviour at lower sizes, l_b=4 nm and below. As shown in Figure 12, instead of shearing the prismatic loop, the glissile dislocation circumvents the l_b=4 nm loop via a climbing process during which several atoms of the prismatic loop are absorbed by the dislocation, leading to the formation of two superjogs, similar to those observed in case #1. This corresponds to an R3 interaction mechanism. Similar results are observed for l_b=3 nm where even more atoms from the prismatic loop are absorbed. Finally, at a critical size of l_b^*=5 nm, both mechanisms occur equally likely by simply changing the seed of atoms starting velocities.

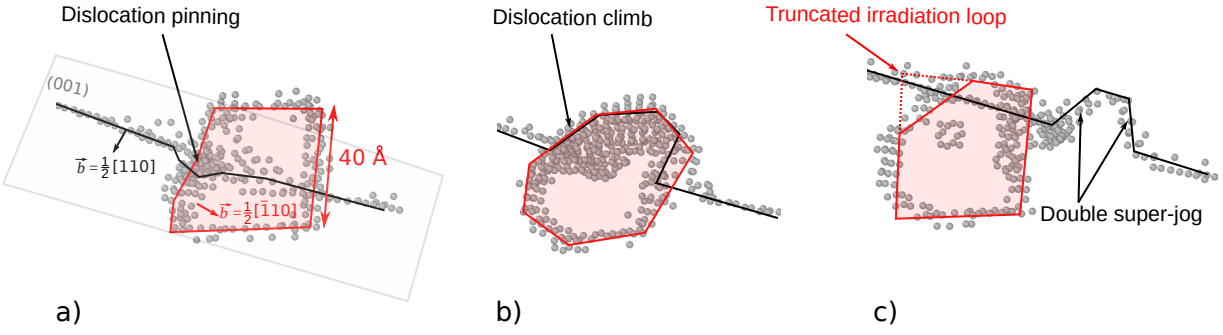

Figure 12: Interaction between a 1/2[110](001) edge dislocation and a 1/2[$\bar{1}$10]($\bar{1}$10) prismatic loop (case #2, β=90°, l_b=40 Å) leading to the formation of two superjogs. (a-c) MD simulation. Dislocation atoms identified using the PTM algorithm are illustrated in grey. Lines and arrows emphasise dislocation lines and Burgers vectors (black=glissile dislocation, red=irradiation loop).

When the prismatic loop is large (l_b>l_b^*), it behaves as four distinct dislocation segments and the interaction (loop shearing without contact reaction) is correctly described by the elastic theory applied to infinite segments. However, smaller loops (l_b<l_b^*) partially lose their dislocation character and behave rather as a cluster of interstitial atoms. In

this case, parts of the cluster can be torn off upon contact with the mobile dislocation. This *corpuscular* behaviour can only be observed in atomistic simulations since DDD is based on the elastic theory. However, we note that it would be possible to implement a local rule in the DDD simulations to force the absorption of smaller loops by gliding dislocations. Finally, it is worth noticing that the l_b^*=5 nm critical loop size estimated here is in the exact same range as the characteristic loop diameter measured in TEM experiments (Onofri et al. 2016). While further experimental analysis would be required to identify the leading interaction process when smaller prismatic loops are involved, the rapid increase of the loop diameter to l_b^*=5 nm and beyond observed in the experiments (Onofri et al. 2016) suggests that the loop shearing mechanism observed for $l_b > l_b^*$ should be active experimentally. Finally, one can mention the influence of the dislocation length on the release of the helical turn (case #4) described in Figures 10 where the competition between the dislocation arm length and the irradiation loop density might influence hardening. More statistics running additional DDD simulations with various dimensions and defect densities might help to predict possible variations in the stress response.

Shovelling and clear bands

Assuming a defect microstructure made of {001} glissile dislocations and randomly distributed {110} irradiation loops, {001} edge dislocations should be more mobile than screw dislocations and should therefore be shorter. Indeed, our simulation results summarised in Table 1 show that the glide of {001} edge dislocation is not significantly hampered by irradiation loops while screw dislocations are strongly pinned by helical turns. This, in addition to the lower elastic line energy of screw dislocations that already favours dislocation extension along the Burgers vector direction, should favour the development of an anisotropic dislocation microstructure made of extended screw dislocation segments and shorter edge segments. As already discussed, multiple helical turns can form along a single screw segment and a shovelling mechanism, during which the dislocation pushes the helical turns along its line to produce long screw segments able to circumvent the helical turns, was observed during case #4 DDD simulations. Also, as in the case of a drag effect, shovelling makes the irradiation loop density spatially heterogeneous and leads to the formation of defect-free clear bands as illustrated in Figure 13.

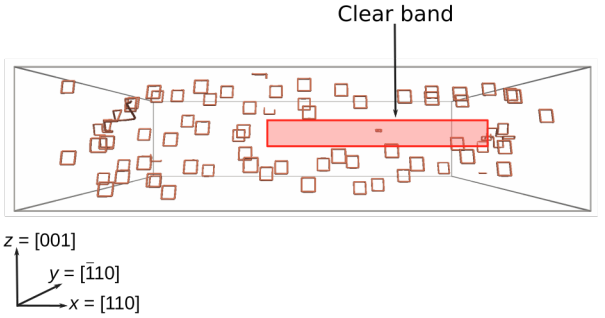

Figure 13: Clear band formation during a DDD simulation at constant shear rate of a screw dislocation gliding through a population of 1/2[$\bar{1}$10]($\bar{1}$10) prismatic loops (case #4, l_b=5 nm, ρ_b=10^{22} m^{-3}).

In the constant shear rate DDD simulation, the clear band already forms after the first passage of the glissile dislocation. So, we can conclude that it should easily form during plastic deformation, leading to plastic localisation and promoting further the deformation of the material. Clear band formation was analysed by Sharp *et al.* in FCC metals using TEM (Sharp 1967). More recently, Robach *et al.* have investigated dislocation-irradiation defect interactions in copper and identified channels cleared of irradiation defects after the passing of screw dislocations (Robach et al. 2003). Finally, Nogaret *et al.* have illustrated the same mechanism using DDD simulations of glissile dislocations interacting with Frank loops in copper (Nogaret et al. 2008). In their work, the authors have shown that the first dislocation passing through the simulation cell was characterised by many pinning points. It was also mostly responsible for the shovelling observed during the simulation, modifying the defect microstructure and allowing the next dislocations to glide more easily, leading to a channelling effect in a band cleared of irradiation defects. The present simulations fully confirm this scenario in UO_2.

In the present case, clear bands can form by both the drag (case #5) and shovelling (cases #4 and #6) of the prismatic loops by screw dislocations. One can assume that edge dislocations will play a limited role because of their shorter lengths. Moreover, only the unpinning from helical turns requires a high stress and thus, irradiation hardening is mostly controlled by this process. Helical turn formation on screw dislocations thus plays a central role in clear band formation and irradiation hardening. The same conclusion was reached in FCC metals (Nogaret et al. 2008), thus confirming the similarities observed between metals and metal oxides in terms of hardening processes happening during irradiation.

Irradiation-hardening modelling

In DDD simulations at constant shear rate, at least two cases (cases #1 and #5) lead to the drag of the prismatic loops induced only by long-range interactions with the glissile dislocations. The DBH model (Equation 2) being only valid in case of 1) contact reactions between dislocations and 2) homogeneously distributed defects, it does not apply to these cases. On the other hand, both configurations are characterised by a dynamical hardening process that can be rationalised using the Orowan's rate equation $\dot{\gamma}_p=\rho_m b_d v(\tau)$, where ρ_m is the mobile dislocation density. Indeed, the stress increase $\Delta\tau$ has shown to be particularly sensitive to the shear rate decreasing from $\Delta\tau$=92 to 15 MPa when the shear rate was decreased from $\dot{\gamma}=10^5$ down to 10^4 s^{-1} in case #1. Also, quantifying hardening in cases where helical turns form (case #4) is particularly complex. In particular, we did verify that case #4 does not follow the DBH model but exhibits a complex behaviour that does not depend only on the loop density ρ_b. Also, it was shown in metals (Rodney 2004) that the unpinning stress of a straight periodic screw dislocation from a helical turn follows the Orowan's stress law, as modified by Scattergood and Bacon (Scattergood and Bacon 1975). However, in the case of a large-scale simulation, the irradiation-defect microstructure evolves during the simulation, which hinders application of Equation 2. Thus, one of the main conclusions of this work is that the strengthening dependence in terms of defect density is not as straightforward as is generally thought and, for those cases, new strain-hardening models accounting for the influence of delocalized and heterogeneous densities of obstacles are required. Finally, case #2 is the only configuration where the dispersed barrier model can be applied although again with some reservation as non-contacting segments pinning the dislocation were also observed in addition to intersecting segments (see Figure 5a). And the corresponding resistance is low, such that we do not expect this reaction to play any significant role in irradiation hardening. Simple irradiation hardening coefficients as obtained using Equation 2 are therefore difficult to derive and probably physically irrelevant because most of the interaction cases between dislocations and irradiation loops do not satisfy the conditions to apply the DBH model (localised defects, homogeneous distribution of defects, *etc.*). From a more global perspective, the strengthening (or softening) induced by the interaction between glissile dislocations and other irradiation defects such as vacancies, Frenkel pairs or fission gas bubbles should be further investigated to provide a fully comprehensive analysis of irradiation-induced hardening in UO_2. This opens the road to the development of new and more versatile hardening models that should help to model the mechanical properties of nuclear materials.

5. Conclusion

This study focused on modelling the interactions of 1/2<110>{001} dislocations with {110} irradiation loops and the induced hardening in the UO_2 fuel using MD and DDD simulations. All configurations depending on the primary dislocation character and prismatic loop orientation were tested and, among others, we identified two cases (screw dislocation *vs.* prismatic loop with parallel and 120° Burgers vectors, case #4 and #6) leading to a particularly strong lock made of an helical turn, similar to those observed in irradiated metals. The formation of hard-pinning configurations confirms the role played by irradiation-induced dislocations on the irradiation hardening of UO_2 fuel in accidental conditions (T=2000 K). Indeed, massive DDD simulations integrating a large population of irradiation loops have shown that the flow stress under constant shear rate might increase by about 2 orders of magnitude, beyond the GPa range, due to the multiplication of helical turn configurations. Furthermore, two mechanisms of loop drag and shovelling were identified as precursors of clear bands (defect-depleted zones) and heterogeneous microstructures of defects, very similar to those observed in irradiated metals. Nevertheless, most of the hardening configurations observed here occur without dislocation contact reactions, which precludes a strict application of the existing DBH model and irradiation-hardening quantification. New hardening models integrating non-local interactions between

dislocations and irradiation defects are required.

6. Acknowledgements

This research is achieved in the framework of a simulation project devoted to the PLEIADES fuel software environment funding by the French nuclear institute between CEA, EDF and FRAMATOME.

References

Alamo, A., J.-M. Lefebvre, and J. Soullard (1978). "Deformation plastique du bioxyde d'uranium: Observation des sous-structures de dislocations". In: *Journal of Nuclear Materials* 75.1, pp. 145–153.

Amodeo, J., P. Carrez, B. Devincre, and P. Cordier (2011). "Multiscale modelling of MgO plasticity". In: *Acta Materialia* 59.6, pp. 2291 –2301.

Amodeo, J., S. Dancette, and L. Delannay (2016). "Atomistically-informed crystal plasticity in MgO polycrystals under pressure". In: *International Journal of Plasticity* 82.C, pp. 177 –191.

Armstrong, D., C. Hardie, J. Gibson, A. Bushby, P. Edmondson, and S. Roberts (2015). "Small-scale characterisation of irradiated nuclear materials: Part II nanoindentation and micro-cantilever testing of ion irradiated nuclear materials". In: *Journal of Nuclear Materials* 462, pp. 374–381.

Arsenlis, A., W. Cai, M. Tang, M. Rhee, T. Oppelstrup, G. Hommes, T. G. Pierce, and V. V. Bulatov (2007). "Enabling strain hardening simulations with dislocation dynamics". In: *Modelling and Simulation in Materials Science and Engineering* 15.6, p. 553.

Arsenlis, A., M. Rhee, G. Hommes, R. Cook, and J. Marian (2012). "A dislocation dynamics study of the transition from homogeneous to heterogeneous deformation in irradiated body-centered cubic iron". In: *Acta Materialia* 60.9, pp. 3748–3757.

Bacon, D., Y. Osetsky, and D. Rodney (2009). "Chapter 88 Dislocation–Obstacle Interactions at the Atomic Level". In: *Dislocations in Solids*. Vol. 15. Elsevier, pp. 1–90.

Baker, C. (1977). "The fission gas bubble distribution in uranium dioxide from high temperature irradiated sghwr fuel pins". In: *Journal of Nuclear Materials* 66.3, pp. 283–291.

Barnett, D. M. (1985). "The displacement field of a triangular dislocation loop". In: *Philosophical Magazine A* 51.3, pp. 383–387.

Baudouin, J.-B., A. Nomoto, M. Perez, G. Monnet, and C. Domain (2015). "Molecular dynamics investigation of the interaction of an edge dislocation with Frank loops in Fe–Ni10–Cr20 alloy". In: *Journal of Nuclear Materials* 465, pp. 301–310.

Borde, M., M. Freyss, E. Bourasseau, B. Michel, D. Rodney, and J. Amodeo (2022). "Atomic-scale modeling of 1/2<110>{001} edge dislocations in UO_2 : core properties and mobility". In: *Journal of Nuclear Materials* 574, p. 154157.

Bulatov, V. V. and W Cai (2006). *Computer Simulations of Dislocations*. Oxford University Press. Oxford University Press.

Byron, J. F. (1968). "The yield and flow of single crystals of uranium dioxide". In: *Journal of Nuclear Materials* 28.1, pp. 110–114.

Cai, W., A. Arsenlis, C. Weinberger, and V. V. Bulatov (2006). "A non-singular continuum theory of dislocations". In: *Journal of the Mechanics and Physics of Solids* 54, pp. 561–587.

Cai, W., V. V. Bulatov, J. Chang, J. Li, and S. Yip (2003). "Periodic image effects in dislocation modelling". In: *Philosophical Magazine* 83.5, pp. 539–567.

Cereceda, D., M. Diehl, F. Roters, D. Raabe, J. M. Perlado, and J. Marian (2016). "Unraveling the temperature dependence of the yield strength in single-crystal tungsten using atomistically-informed crystal plasticity calculations". In: *International Journal of Plasticity* 78, pp. 242–265. eprint: 1506.02224.

Chartier, A., C. Onofri, L. Van Brutzel, C. Sabathier, O. Dorosh, and J. Jagielski (2016). "Early stages of irradiation induced dislocations in urania". In: *Applied Physics Letters* 109.18, p. 181902.

Cui, Y., G. Po, and N. M. Ghoniem (2018). "A coupled dislocation dynamics-continuum barrier field model with application to irradiated materials". In: *International Journal of Plasticity* 104, pp. 54–67.

Cui, Y., E. Aydogan, J. G. Gigax, Y. Wang, A. Misra, S. A. Maloy, and N. Li (2021). "In Situ Micro-Pillar Compression to Examine Radiation-Induced Hardening Mechanisms of FeCrAl Alloys". In: *Acta Materialia* 202, pp. 255–265.

Das, S., H. Yu, K. Mizohata, E. Tarleton, and F. Hofmann (2020). "Modified deformation behaviour of self-ion irradiated tungsten: A combined nano-indentation, HR-EBSD and crystal plasticity study". In: *International Journal of Plasticity* 135, p. 102817. eprint: 1911.10397.

Drouet, J., L. Dupuy, F. Onimus, F. Mompiou, S. Perusin, and A. Ambard (2014). "Dislocation dynamics simulations of interactions between gliding dislocations and radiation induced prismatic loops in zirconium". In: *Journal of Nuclear Materials* 449.1-3, pp. 252–262.

Erel, C., G. Po, T. Crosby, and N. Ghoniem (2017). "Generation and interaction mechanisms of prismatic dislocation loops in FCC metals". In: *Computational Materials Science* 140, pp. 32–46.

Fossati, P., L. Van Brutzel, and B. Devincre (2013). "Molecular dynamics simulation of dislocations in uranium dioxide". In: *Journal of Nuclear Materials* 443.1-3, pp. 359–365.

Frazer, D and P. Hosemann (2019). "Plasticity of UO2 studied and quantified via elevated temperature micro compression testing". In: *Journal of Nuclear Materials* 525, pp. 140–144.

Frazer, D., B. Shaffer, B. Gong, P. Peralta, J. Lian, and P. Hosemann (2021). "Elevated temperature nanoindentation creep study of plastically deformed and spark plasma sintered UO2". In: *Journal of Nuclear Materials* 545, p. 152605.

Ghoniem, N., S.-H. Tong, B. Singh, and L. Sun (2001). "On dislocation interaction with radiation-induced defect clusters and plastic flow localization in fcc metals". In: *Philosophical Magazine A* 81.11, pp. 2743–2764.

He, L. F., J. Pakarinen, M. A. Kirk, J. Gan, A. T. Nelson, X. M. Bai, A. El-Azab, and T. Allen (2014). "Microstructure evolution in Xe-irradiated UO_2 at room temperature". In: *Nuclear Instruments and Methods in Physics Research Section B: Beam Interactions with Materials and Atoms* 330, pp. 55–60.

Henderson, A., J. Ahrens, and C. Law (2004). *The ParaView Guide*. Vol. 366. Kitware Clifton Park, NY.

Hirel, P. (2015). "Atomsk: A tool for manipulating and converting atomic data files". In: *Computer Physics Communications* 197, pp. 212–219.

Jackson, R. A., A. D. Murray, J. H. Harding, and C. R. A. Catlow (1986). "The calculation of defect parameters in UO_2". In: *Philosophical Magazine A* 53.1, pp. 27–50.

Jonnet, J., P. V. Uffelen, T. Wiss, D. Staicu, B. Rémy, and J. Rest (2008). "Growth mechanisms of interstitial loops in -doped UO2 samples". In: *Nuclear Instruments and Methods in Physics Research Section B: Beam Interactions with Materials and Atoms* 266.12-13, pp. 3008–3012.

Keller, R. J., T. E. Mitchell, and A. H. Heuer (1988a). "Plastic deformation in nonstoichiometric UO_{2+x} single crystals—I. Deformation at low temperatures". In: *Acta metallurgica* 36.4, pp. 1061–1071.

— (1988b). "Plastic deformation in nonstoichiometric UO_{2+x} single crystals—II. Deformation at high temperatures". In: *Acta metallurgica* 36.4, pp. 1073–1083.

Kubin, L. P. (2013). *Dislocations, mesoscale simulations and plastic flow*. Oxford Materials. Oxford Series on Materials Modelling. Ed. Oxford.

Larsen, P. M., S. Schmidt, and J. Schiøtz (2016). "Robust structural identification via polyhedral template matching". In: *Modelling and Simulation in Materials Science and Engineering* 24.5, p. 055007.

Le Prioux, A., P. Fossati, S. Maillard, T. Jourdan, and P. Maugis (2016). "Empirical potential simulations of interstitial dislocation loops in uranium dioxide". In: *Journal of Nuclear Materials* 479, pp. 576–584.

Lefèbvre, J.-M., J. Soullard, R.-J. Gaboriaud, and J. Grilhé (1976). "Calcul d'energie de fautes d'empilement dans le dioxyde d'uranium". In: *Journal of Nuclear Materials* 60.1, pp. 59–65.

Li, D., H. Zbib, X. Sun, and M. Khaleel (2014). "Predicting plastic flow and irradiation hardening of iron single crystal with mechanism-based continuum dislocation dynamics". In: *International Journal of Plasticity* 52, pp. 3–17.

Li, Y., M. Boleininger, C. Robertson, L. Dupuy, and S. L. Dudarev (2019). "Diffusion and interaction of prismatic dislocation loops simulated by stochastic discrete dislocation dynamics". In: *Physical Review Materials* 3.7, p. 073805.

Lindroos, M., N. Vajragupta, J. Heikinheimo, D. R. Costa, A. Biswas, T. Andersson, and P. Olsson (2023). "Micromechanical modeling of single crystal and polycrystalline UO2 at elevated temperatures". In: *Journal of Nuclear Materials* 573, p. 154127.

Liu, B., D. Raabe, P. Eisenlohr, F. Roters, A. Arsenlis, and G. Hommes (2011). "Dislocation interactions and low-angle grain boundary strengthening". In: *Acta Materialia* 59.19, pp. 7125–7134.

Liu, X.-Y., E. Martinez, and B. P. Uberuaga (2019). "Dissociated vacancies and screw dislocations in MgO and UO2: atomistic modeling and linear elasticity analysis". In: *Scientific reports* 9.1, pp. 1–9.

Lunev, A., A. Kuksin, and S. Starikov (2017). "Glide mobility of the 1/2[110](001) edge dislocation in UO_2 from molecular dynamics simulation". In: *International Journal of Plasticity* 89, pp. 85–95.

Lunev, A., S. Starikov, T. Aliev, and V. Tseplyaev (2018). "Understanding thermally-activated glide of 1/2<110>{110} screw dislocations in UO_2 – A molecular dynamics analysis". In: *International Journal of Plasticity* 110, pp. 294–305.

Madec, R., B. Devincre, L. P. Kubin, T. Hoc, and D. Rodney (2003). "The Role of Collinear Interaction in Dislocation-Induced Hardening". In: *Science* 301.5641, pp. 1879–1882.

Madec, R., L. Portelette, B. Michel, and J. Amodeo (2023). "Plastic anisotropy and composite slip: Application to uranium dioxide". In: *Acta Materialia* 255, p. 119016.

Martin, G., P. Garcia, C. Sabathier, L. Van Brutzel, B. Dorado, F. Garrido, and S. Maillard (2010). "Irradiation-induced heterogeneous nucleation in uranium dioxide". In: *Physics Letters A* 374.30, pp. 3038–3041.

Messerschmidt, U. (2010). *Dislocation dynamics during plastic deformation*. Ed. by R Hull, C Jagadish, R. M. o. Jr, J Parisi, Z Wang, and H Warlimont. Vol. 129. Springer Series in Materials Science. Springer Series in Materials Science.

Michel, B., C. Nonon, J. Sercombe, F. Michel, and V. Marelle (2013). "Simulation of Pellet-Cladding Interaction with the PLEIADES Fuel Performance Software Environment". In: *Nuclear Technology* 182.2, pp. 124–137.

Monnet, G. (2018). "Multiscale modeling of irradiation hardening: Application to important nuclear materials". In: *Journal of Nuclear Materials* 508, pp. 609–627.

Naamane, S, G Monnet, and B Devincre (2010). "Low temperature deformation in iron studied with dislocation dynamics simulations". In: *International Journal of Plasticity* 26.1, pp. 84 –92.

Nadeau, J. S. (1969). "Dependence of Flow Stress on Nonstoichiometry in Oxygen-Rich Uranium Dioxide at High Temperatures". In: *Journal of the American Ceramic Society* 52.1, pp. 1–7.

Nogaret, T., D. Rodney, M. Fivel, and C. Robertson (2008). "Clear band formation simulated by dislocation dynamics: Role of helical turns and pile-ups". In: *Journal of Nuclear Materials* 380.1-3, pp. 22–29.

Nordlund, K. (2019). "Historical review of computer simulation of radiation effects in materials". In: *Journal of Nuclear Materials* 520, pp. 273–295.

Onofri, C., M. Legros, J. Léchelle, H. Palancher, C. Baumier, C. Bachelet, and C. Sabathier (2017). "Full characterization of dislocations in ion-irradiated polycrystalline UO_2". In: *Journal of Nuclear Materials* 494, pp. 252–259.

Onofri, C., C. Sabathier, C. Baumier, C. Bachelet, D. Drouan, M. Gérardin, and M. Legros (2020). "Extended defect change in UO_2 during in situ TEM annealing". In: *Acta Materialia* 196, pp. 240–251.

Onofri, C., C. Sabathier, H. Palancher, G. Carlot, S. Miro, Y. Serruys, L. Desgranges, and M. Legros (2016). "Evolution of extended defects in polycrystalline UO_2 under heavy ion irradiation: combined TEM, XRD and Raman study". In: *Nuclear Instruments and Methods in Physics Research Section B: Beam Interactions with Materials and Atoms* 374, pp. 51–57.

Osetsky, Y. N., D. Rodney, and D. J. Bacon (2006). "Atomic-scale study of dislocation–stacking fault tetrahedron interactions. Part I: mechanisms". In: *Philosophical Magazine* 86.16, pp. 2295–2313.

Osetsky, Y. and D. Bacon (2012). "Atomic-level level dislocation dynamics in irradiated metals". In: *Comprehensive Nuclear Materials* 1, 1b23.

Panetier, C., Y. Pipon, C. Gaillard, D. Mangin, J. Amodeo, J. Morthomas, T. Wiss, A. Benedetti, R. Ducher, R. Dubourg, and N. Moncoffre (2022). "Cs diffusion mechanisms in UO2 investigated by SIMS, TEM, and atomistic simulations". In: *The Journal of Chemical Physics* 156.4, p. 044705.

Portelette, L., J. Amodeo, R. Madec, J. Soulacroix, T. Helfer, and B. Michel (2018). "Crystal viscoplastic modeling of UO_2 single crystal". In: *Journal of Nuclear Materials* 510, pp. 635–643.

Portelette, L., J. Amodeo, B. Michel, and R. Madec (2020). "Athermal dislocation strengthening in UO_2". In: *Journal of Nuclear Materials* 538, p. 152157.

Potashnikov, S., A. Boyarchenkov, K. Nekrasov, and A. Kupryazhkin (2011). "High-precision molecular dynamics simulation of UO_2–PuO_2: Pair potentials comparison in UO_2". In: *Journal of Nuclear Materials* 419.1-3, pp. 217–225.

Robach, J., I. Robertson, B. Wirth, and A. Arsenlis (2003). "In-situ transmission electron microscopy observations and molecular dynamics simulations of dislocation-defect interactions in ion-irradiated copper". In: *Philosophical Magazine* 83.8, pp. 955–967.

Rodney, D. (2004). "Molecular dynamics simulation of screw dislocations interacting with interstitial frank loops in a model FCC crystal". In: *Acta Materialia* 52.3, pp. 607–614.

Rodney, D. and G. Martin (1999). "Dislocation pinning by small interstitial loops: A molecular dynamics study". In: *Physical Review Letters* 82.16, pp. 3272 –3275.

Rodney, D. and L. Proville (2009). "Stress-dependent Peierls potential: Influence on kink-pair activation". In: *Physical Review B* 79.9, pp. 1 –9.

Rodney, D., L. Ventelon, E. Clouet, L. Pizzagalli, and F. Willaime (2017). "Ab initio modeling of dislocation core properties in metals and semiconductors". In: *Acta Materialia* 124, pp. 633–659.

Saleh, M., Z. Zaidi, M. Ionescu, C. Hurt, K. Short, J. Daniels, P. Munroe, L. Edwards, and D. Bhattacharyya (2016). "Relationship between damage and hardness profiles in ion irradiated SS316 using nanoindentation – Experiments and modelling". In: *International Journal of Plasticity* 86, pp. 151–169.

Sawbridge, P. T. and E. C. Sykes (1971). "Dislocation glide in UO $_2$ single crystals at 1600°K". In: *Philosophical Magazine* 24.187, pp. 33–53.

Scattergood, R. and D. J. Bacon (1975). "The Orowan mechanism in anisotropic crystals". In: *Philosophical Magazine A* 31, p. 179.

Seeger, A. (1958). "Proceedings of the 2nd International Conference on Peaceful Uses of Atomic Energy, Geneva, Switzerland". In: *Basic Metallurgy and Fabrication of Fuels*, pp. 1–13.

Sharp, J. (1967). "Deformation of neutron-irradiated copper single crystals". In: *Philosophical Magazine* 16.139, pp. 77–96.

Shi, X., L. Dupuy, B. Devincre, D. Terentyev, and L. Vincent (2015). "Interaction of <100> dislocation loops with dislocations studied by dislocation dynamics in α-iron". In: *Journal of Nuclear Materials* 460, pp. 37–43.

Skelton, R. and A. M. Walker (2017). "Peierls-Nabarro modeling of dislocations in UO_2". In: *Journal of Nuclear Materials* 495, pp. 202–210.

Sonoda, T., M. Kinoshita, I. Ray, T. Wiss, H. Thiele, D. Pellottiero, V. Rondinella, and H. Matzke (2002). "Transmission electron microscopy observation on irradiation-induced microstructural evolution in high burn-up UO_2 disk fuel". In: *Nuclear Instruments and Methods in Physics Research Section B: Beam Interactions with Materials and Atoms* 191.1-4, pp. 622–628.

Soulié, A., J.-P. Crocombette, A. Kraych, F. Garrido, G. Sattonnay, and E. Clouet (2018). "Atomistically-informed thermal glide model for edge dislocations in uranium dioxide". In: *Acta Materialia* 150, pp. 248–261.

Stukowski, A. (2009). "Visualization and analysis of atomistic simulation data with OVITO–the Open Visualization Tool". In: *Modelling and simulation in materials science and engineering* 18.1, p. 015012.

Thompson, A. P., H. M. Aktulga, R. Berger, D. S. Bolintineanu, W. M. Brown, P. S. Crozier, P. J. in 't Veld, A. Kohlmeyer, S. G. Moore, T. C. Nguyen, R. Shan, M. J. Stevens, J. Tranchida, C. Trott, and S. J. Plimpton (2022). "LAMMPS - a flexible simulation tool for particle-based materials modeling at the atomic, meso, and continuum scales". In: *Computer Physics Communications* 271, p. 108171.

Van Brutzel, L., A. Chartier, and J.-P. Crocombette (2008). "Basic mechanisms of Frenkel pair recombinations in UO_2 fluorite structure calculated by molecular dynamics simulations". In: *Physical Review B* 78.2, p. 024111.

Weygand, D., L. H. Friedman, E. Van Der Giessen, and A. Needleman (2002). "Aspects of boundary-value problem solutions with three-dimensional dislocation dynamics". In: *Modelling and Simulation in Materials Science and Engineering* 10.4, pp. 437–468.

Whapham, A. D. (1966). "Electron Microscope Observation of the Fission-Gas Bubble Distribution in UO_2". In: *Nuclear Applications* 2.2, pp. 123–130.

Ye, B., M. A. Kirk, W. Chen, A. Oaks, J. Rest, A. Yacout, and J. F. Stubbins (2011). "TEM investigation of irradiation damage in single crystal CeO_2". In: *Journal of Nuclear Materials* 414.2, pp. 251–256.

Yust, C. S. and C. J. McHargue (1969). "Dislocation substructures in deformed uranium dioxide single crystals". In: *Journal of nuclear materials* 31.2, pp. 121–137.

Zbib, H. M., T. D. De La Rubia, M. Rhee, and J. P. Hirth (2000). "3D dislocation dynamics: stress–strain behavior and hardening mechanisms in fcc and bcc metals". In: *Journal of Nuclear Materials* 276.1-3, pp. 154–165.

Zinkle, S. and G. Was (2013). "Materials challenges in nuclear energy". In: *Acta Materialia* 61.3, pp. 735–758.